Bifurcation structure of traveling pulses in type-I excitable media

Pablo Moreno-Spiegelberg,[1] Andreu Arinyo-i-Prats,[2] Daniel Ruiz-Reynés,[3] Manuel A. Matias,[1] and Damià Gomila[1,*]

[1]IFISC (CSIC-UIB), Instituto de Física Interdisciplinar y Sistemas Complejos, E-07122 Palma de Mallorca, Spain
[2]Institute of Computer Science, Czech Academy of Sciences, 182 07 Prague 8, Czech Republic
[3]Laboratory of Dynamics in Biological Systems, Department of Cellular and Molecular Medicine, University of Leuven (KU Leuven), B-3000 Leuven, Belgium

(Received 18 February 2022; accepted 1 August 2022; published 15 September 2022)

We study the scenario in which traveling pulses emerge in a prototypical type-I one-dimensional excitable medium, which exhibits two different routes to excitable behavior, mediated by a homoclinic (saddle-loop) and a saddle-node on the invariant cycle bifurcations. We characterize the region in parameter space in which traveling pulses are stable together with the different bifurcations behind either their destruction or loss of stability. In particular, some of the bifurcations delimiting the stability region have been connected, using singular limits, with the two different scenarios that mediated type-I local excitability. Finally, the existence of traveling pulses has been linked to a drift pitchfork instability of localized steady structures.

DOI: 10.1103/PhysRevE.106.034206

I. INTRODUCTION

Excitable dynamical systems have a linearly stable rest state (i.e., a stable fixed point) that, under nonlinear perturbations above a certain amplitude, experience a long excursion in phase space. Excitable media are dynamical systems extended in space that are locally excitable, and so perturbations of the rest state may propagate in the system. This is because a local perturbation that excites an excursion in phase space can trigger an excitable excursion of the nearest-neighbor points to finally return back to the rest state. In one dimension (1-D), the result of this process is the creation of a traveling pulse (TP). After a pulse passes through, the system returns (locally) to the rest state, becoming susceptible to be excited again and, therefore, TPs can pass many times through the same region, leading to a huge variety of spatiotemporal structures, such as solitary pulses, wave trains, and, in two dimensions (2-D), target patterns or rotating spirals [1–4]. Two ingredients are essential to observe these dynamic regimes: on one hand, temporal excitability of the local dynamics; on the other hand, a spatial coupling between the elements of the system to allow a perturbation to propagate in space.

Temporal excitability is usually associated with the sudden destruction of a large amplitude limit cycle. Remnant traces of this cycle in phase space constitute the excitable excursion. The bifurcation through which the limit cycle is destroyed leads to differences in the excitable trajectory and, therefore, unique properties of the excitable system. Temporal excitability can be classified into two types, I and II, depending on which kind of bifurcation mediates the transition to the limit cycle [5–7].

Type-I excitability is generated at a saddle-node on invariant cycle (SNIC) or homoclinic (also known as saddle-loop) bifurcations, involving a saddle point aside from the stable rest point [7]. It has been profusely reported in neuroscience [7] and also in other fields [8–10]. More generally, type-I excitable behavior can be found in the case that the excitable system is defined in a higher-dimensional phase space, as is the case of three-variable excitable systems exhibiting a homoclinic to a saddle-focus, instead of a saddle, i.e., a Shilnikov scenario, that leads to multipulse excitability [11–13]. In turn, type-II excitability is well explained in textbooks with a neuroscience orientation [7,14] and is the type of excitability found in the well-known FitzHugh-Nagumo model. Type-II is mediated by a Hopf bifurcation that creates very large stable cycle in a very narrow parameter space. Typically, this corresponds to a supercritical Hopf followed by a canard [15], i.e., a sudden growth of the cycle happening in fast-slow systems, or to a subcritical Hopf with a fold of cycles. In turn, each bifurcation confers to type-I and type-II excitabilities unique and distinct features.

In general, in type-I excitability, (i) the distance between the stable rest point and the saddle defines a threshold in phase space, given by the stable manifold of the saddle, and (ii) the duration of an excitable excursion depends on how close the initial condition is to the threshold, diverging for initial conditions on it.

In type-II excitability instead, (i) there is not a well-defined threshold in phase space, but a narrow region of initial condition produces a pseudothreshold. The thickness of this region depends on the ratio between the timescales of the system. Hence, the excitability is only well defined when the difference in timescales is large enough. (ii) The differences in temporal scales provide trajectories with a well-defined duration determined by the slow dynamics, independently of the initial condition.

We will coin type-I (type-II) excitable media to the space extended system obtained by adding diffusion to a type-I (type-II) excitable system. Since type-I and type-II excitability are intrinsically different, it is expected to find some differences between type-I and type-II excitable media. The

*damia@ifisc.uib-csic.es

traveling pulses found in both kinds of media share some general features. In both cases, TPs are isolated, having speed and shape not determined by the initial conditions, and annihilate when they collide with other pulses. Nevertheless, the mechanisms behind the creation and stabilization of the TP (and the behavior of the pulse close to these points) depend on the associated temporal excitability. Also, the shape of TP may quite differ depending on the type of excitability. For instance, type-II excitable pulses in systems with a big timescale separation have a distinctive square-like form which is not observed in the type-I case.

Until quite recently, most studies of excitable media have been carried out in the case that the excitable medium is locally of type-II, using models that have the corresponding bifurcations in the local dynamics [1,2]. These include examples in neuroscience [16], depression waves [17], cardiac tissue [4], reaction-diffusion systems [18], and nonlinear optics [19]. The origin of the TPs in these systems can be tracked to the singular limit when the difference between timescales diverges [1,2]. This mechanism is strongly related with the bifurcations associated with the type-II excitability of the local part.

Nevertheless, there is a number of recent studies in the context of vegetation dynamics [20–23] that report excitable behavior where the local dynamics exhibits features indicating that they are of type-I. Similar behaviors have also been found in other biological systems [16,24]. In some of these systems the origin of the TP is associated with a T-point bifurcation [24,25]. However, the relation between the temporal (local) bifurcations of the system and its spatial structure counterpart (in the case of TPs) has not been properly analyzed in the literature. Connecting a spatially extended system to its local dynamics is a powerful approach. This concept has been successfully applied to explain the emergence of chaos, stationary pulses, and kink patterns in conserved reaction diffusion systems [26,27].

In Ref. [28] we discussed the existence and properties of 1-D TPs in the simplest general model for type-I excitable media we are aware of that exhibits both SNIC and homoclinic bifurcations and showed how the shape of TPs was affected by the proximity in the parameter space to the bifurcations leading to type-I excitability. In this work, we extend this analysis by describing the full bifurcation diagram and dynamical regimes of TPs in type-I excitable media. First, we fully characterize the different bifurcations delimiting the stable region of excitable traveling pulses. We explicitly show the connection between some of the bifurcations of the temporal system and the spatiotemporal dynamics, as was suggested in Ref. [28]. Furthermore, we investigate and characterize bifurcations that are intrinsically spatiotemporal, i.e., with no purely temporal counterpart. Finally, the existence of TPs has been tracked outside the excitable region, until their creation point, connecting excitable traveling pulses with a drift pitchfork bifurcation of localized steady solutions of bistable systems.

The paper is structured as follows: In Sec. II we describe the model we analyze. In Sec. III we characterize the excitable pulses, introduce its stability region, and show the scenarios found when abandoning this region through the different bifurcations. In Sec. IV we analyze in detail the bifurcations that delimite the stability region and connect some of them with spaceless counterparts. In Sec. V we find that the traveling pulses emerge, outside the stability region, from localized steady structures through a Drift Pitchfork bifurcation. Finally, in Sec. VI we give some concluding remarks.

II. MODEL

We consider a general reaction-diffusion model given by the following system of partial differential equations (PDEs):

$$\partial_t u = v + \partial_{xx} u,$$
$$\partial_t v = -u^3 + \mu_2 u + \mu_1 + v(\nu + bu - u^2) + \partial_{xx} v. \quad (1)$$

The local dynamics of the system is described by the bounded normal form of a codimension-three degenerate Takens-Bogdanov bifurcation with triple equilibrium [29]. This is the simplest continuous model which gives a complete description of type-I excitability, in the sense that the excitable region is accessible either through a homoclinic or a SNIC bifurcation. We have added 1-D diagonal diffusion to study spatial propagation. The diffusion coefficients have been chosen to be equal in both fields, and without loss of generality, they have been fixed to one. This choice does not introduce any special symmetry, nor generates spatial instabilities of the homogeneous solutions. We have also checked that slightly different diffusion constants in each field does not substantially modify the results of this work. We fix the parameters $\nu = 1$, $b = 2.4$ and consider μ_1 and μ_2 as control parameters [28].

Excitable pulses in PDEs can be studied using two different approaches. The first approach is the local dynamical system, which describes the evolution of the system without diffusion or, alternatively, the evolution of homogeneous solutions of the system. Excitable pulses somehow transcribe local dynamics in space, resembling in their profile the excitable trajectory in time [28]. Furthermore, the bifurcation behind the creation of excitable trajectories in the local dynamical system is connected with the creation of excitable pulses in the PDEs, as will be expanded in Sec. IV. The second approach is the moving spatial dynamical system, which describes the spatial profile of structures that propagates with a fixed velocity c without changing shape. From this approach, TPs are interpreted as trajectories in a system of ordinary differential equations. Therefore, the creation of TPs can be studied through the bifurcations that generate homoclinic trajectories. In the limit $c \to \infty$, the local dynamical equations are recovered from the moving spatial dynamical system, as shown in Sec. II B, connecting both approaches.

A. Local dynamics

The dynamics of the local system is described by the following set of ordinary differential equations:

$$\frac{du}{dt} = v, \quad \frac{dv}{dt} = -u^3 + \mu_2 u + \mu_1 + v(\nu + bu - u^2). \quad (2)$$

A schematic phase diagram showing the different bifurcations and dynamical regions is shown in Fig. 1 for $\nu = 1$ and $b = 2.4$. The actual phase diagram is shown in Fig. 2.

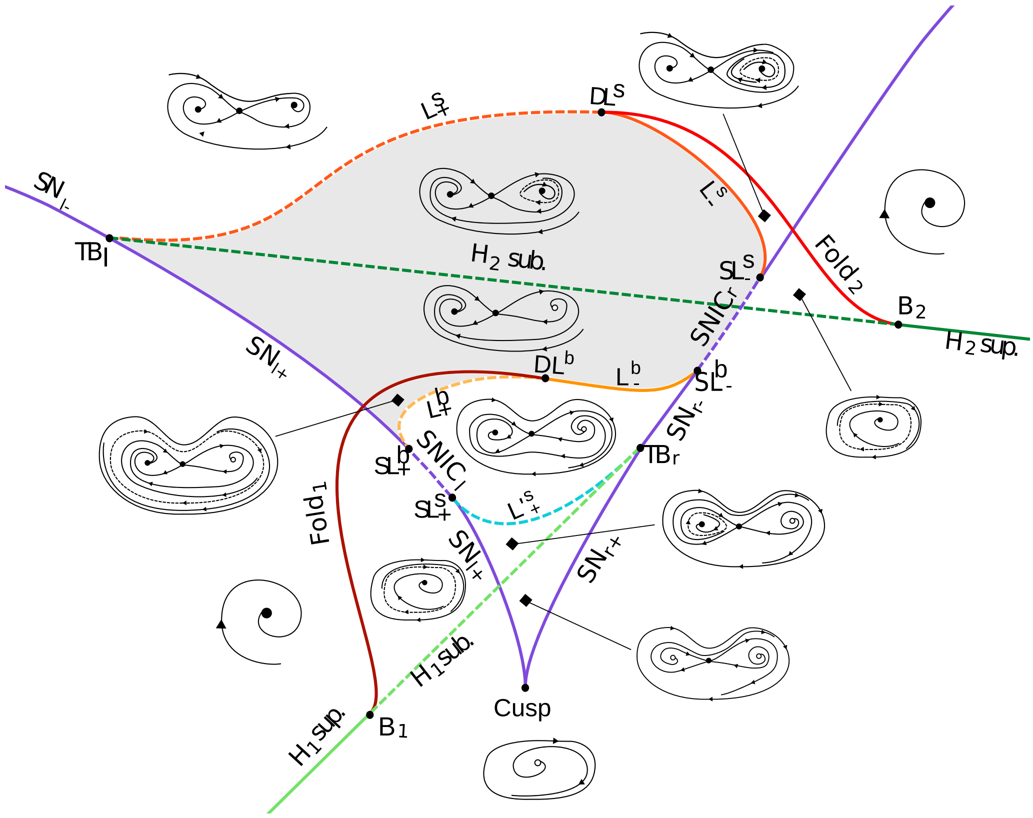

FIG. 1. Schematic phase diagram for the μ_1, μ_2 plane for fixed $\nu = 1$, $b = 2.4$ parameters of equation (2). The lines represent the bifurcations that separate the parameter space in qualitative different behavior of the system. The dots mark the codimension-two points. The diagrams show a schematic representation of the phase portrait in the different regions. Gray area marks the excitability region.

The fixed points of this temporal system are $v^\star = 0$ and $u^\star$ being determined by the solutions to the cubic equation

$$-u^{*3} + \mu_2 u^* + \mu_1 = 0, \tag{3}$$

which represents the unfolding of a cusp bifurcation point located at $\mu_1 = \mu_2 = 0$ (see Fig. 1). Two saddle-node bifurcation lines start from this point and are given by

$$\text{SN}_l: \quad \mu_1 = -2\sqrt{\frac{\mu_2^3}{27}}, \quad \mu_2 > 0,$$

$$\text{SN}_r: \quad \mu_1 = +2\sqrt{\frac{\mu_2^3}{27}}, \quad \mu_2 > 0. \tag{4}$$

In Fig. 1 we attach a plus or a minus to the saddle-node (SN) labels depending on whether they create two unstable fixed points or a saddle and a stable fixed point. These SN bifurcations separate the parameter space in two regions. In the inner region, where the cubic has three real roots, the system has three fixed points: $\{P_i(u_i^*, v^* = 0),\ i = 1, 2, 3\}$ where u_i^* are the roots of Eq. (3) and $u_1^* < u_2^* < u_3^*$. In the outer region the system has a single fixed point $P_0(u_0^*, v^* = 0)$ because u_0^* is the only root of Eq. (3).

A linear stability analysis provides the eigenvalues of the fixed points of (2), given by

$$\lambda_\pm(P_i) = \lambda_\pm(u_i^*) = \frac{\tau(u_i^*) \pm \sqrt{\tau^2(u_i^*) - 4\Delta(u_i^*)}}{2}, \tag{5}$$

where $\tau(u_i^*)$ and $\Delta(u_i^*)$ are the trace and determinant of the Jacobian at P_i given by

$$\tau(u_i^*) = \nu + bu_i^* - u_i^{*2}, \tag{6}$$

$$\Delta(u_i^*) = 3u_i^{*2} - \mu_2. \tag{7}$$

Attending to the eigenvalues, the point P_2 is always a saddle while P_0, P_1, and P_3 can be, depending on the parameters, either foci or nodes.

On the SN_l (SN_r) bifurcation line, the fixed points P_2 and P_3 (P_2 and P_1) collide in a saddle-node point and are annihilated. The point P_1 (P_3) is not affected by this bifurcation and is renamed to P_0 in the outside region.

For the values of ν and b used in this paper, the solutions P_0, P_1, and P_3 can change their stability through Andronov-Hopf bifurcations. Two different Hopf bifurcation lines have been found. One affecting P_1, label as H_1; and another one which involves P_3, label as H_2. Outside the bistable region, both bifurcations lines affect the stability of P_0. These bifurcations are located at

$$\mu_1 = u_{H1,2}^3 - \mu_2 u_{H1,2}, \quad \mu_2 < 3u_{H1,2}^2, \tag{8}$$

where $u_{H1,2}$ is the value of the steady homogeneous solution at the bifurcation

$$u_{H1,2} = \frac{b \pm \sqrt{b^2 + 4\nu}}{2}, \tag{9}$$

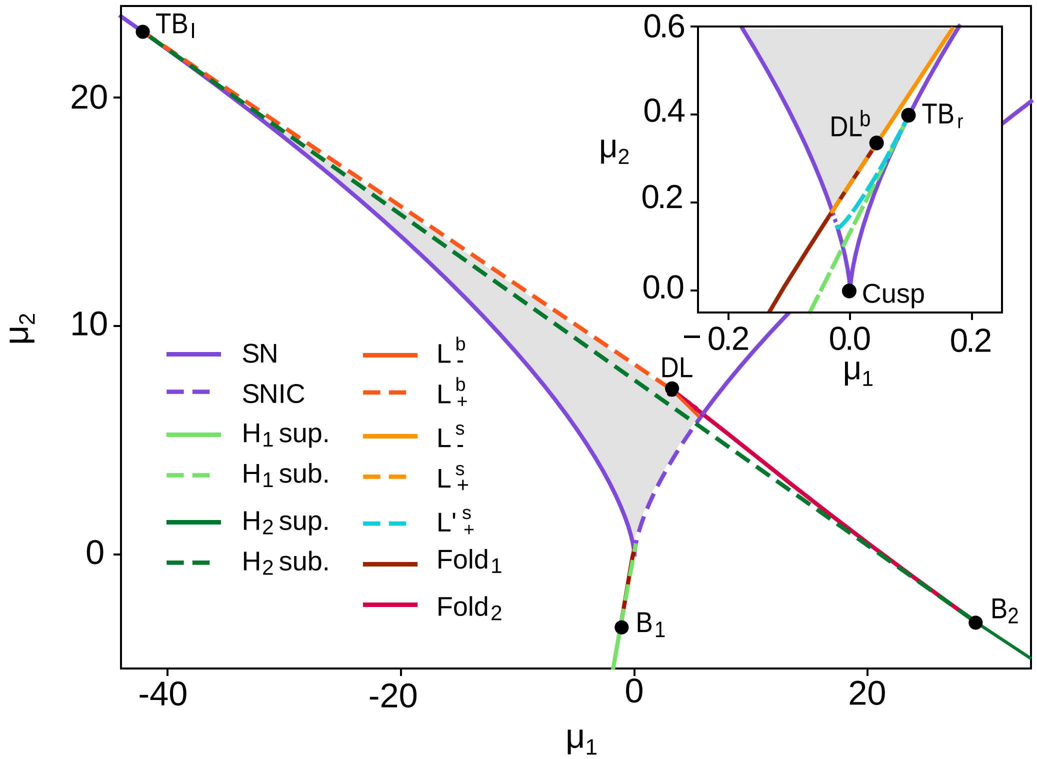

FIG. 2. Actual phase diagram of the temporal system (2) for $\nu = 1$ and $b = 2.4$.

with u_{H1} being the one with a minus sign and u_{H2} the one with a plus sign.

These Hopf bifurcations are subcritical for $\mu_2 > 6bu_{H1,2} - 9u_{H1,2}^2$. The point where the Hopf bifurcation change from super to subcritical, $(\mu_1, \mu_2) = (10u_{H1,2}^3 - 6bu_{H1,2}^2, 6bu_{H1,2} - 9u_{H1,2}^2)$, is known as Bautin point (B), or also degenerate Hopf. From each of the Bautin points emerges, tangentially to the Hopf, a fold of cycles, also known as saddle node of periodic orbits. Although the fold of cycles curve cannot be analytically found, we have obtained a numerical approximation of several points of the fold of cycles associated with H_1 (Fold_1) and the fold associated with H_2 (Fold_2), as can be seen in Fig. 2.

The Fold_1 line ends in a "big" degenerate loop point (DL^b) where the degenerate cycle created at the fold becomes a Homoclinic connection of the P_2 fixed point surrounding P_1 and P_3. The term big denotes that the created cycle surrounds the three fixed points. From this DL^b point starts, tangentially to Fold_1, two big homoclinic bifurcations ($\text{L}^b_\pm$). At the L^b_+ (L^b_-) an unstable (stable) limit cycle is created from a Homoclinic connection of the P_2 fixed point, embracing the three fixed points. The L^b_+ (L^b_-) meets tangentially the SN_l (SN_r) curve in a saddle-node separatrix-loop codimension-two point that we call SL^b_+ (SL^b_-).

The Fold_2 line ends in a "small" degenerate loop point (DL^s) where the degenerate cycle created at the fold becomes a homoclinic connection of P_2 surrounding P_3. The term small denotes that the created cycle surrounds only one fixed point. From this point two small homoclinic bifurcations ($\text{L}^s_\pm$) start tangentially to the Fold_2 line. At the L^s_+ (L^s_-) line an unstable (stable) limit cycle is created from a homoclinic connection of P_2, surrounding just P_3. The L^s_- line ends in a saddle-node separatrix-loop codimension-two point (SL^s_+) where it meets tangentially the SN_r. The L^s_+ curve ends in a Takens-Bogdanov codimension-two point (TB_l) tangentially to the H_2 and the SN_l curves.

The H_1 (H_2) line meets tangentially with the SN_r (SN_l) curve in a Takens-Bogdanov codimension-two point, TB_r (TB_l), at

$$\mu_1 = -2u_{H1,2}^3, \quad \mu_2 = 3u_{H1,2}^2. \tag{10}$$

From each TB point, a small homoclinic bifurcation starts tangentially to the Hopf and SN lines. At these curves, the cycle created in the Andronov-Hopf bifurcation collides with the saddle fixed point and is destroyed. On one hand, the homoclinic arising from TB_r (L'^s_-) ends tangentially to SN_l in the saddle-node separatrix-loop codimension-two point (SL^s_+). On the other hand, the homoclinic arising from TB_l corresponds with the L^s_+ curve mentioned before.

Between the points SL^b_+ and SL^s_+ (SL^b_- and SL^s_-) the SN_r (SN_l) bifurcation line creates a stable (unstable) limit cycle, when crossed in the one-fixed-point direction, in an infinite period bifurcation known as a saddle node on the invariant cycle SNIC_r (SNIC_l).

In the region delimited by the SN_{l+}, $\text{L}^b_\pm$, SNIC_r, and $\text{L}^s_\pm$, shaded in gray in Figs. 1 and 2, the system displays type-I excitable behavior. While the system is in the stable fixed point P_1, a perturbation that moves the system away from the fixed point and below the stable manifold of the P_2 decays exponentially. However, a perturbation that sets the system above this separatrix, grows, making the system explore the remnants of the cycle on a long excursion in phase space, an excitable trajectory, to return afterwards to the rests state P_1.

B. Spatial dynamics in a moving reference frame

To interpret some of the bifurcations involved in the creations of the pulses, it is useful to use a different theoretical framework to complement the PDEs (1). As pulses are steady structures that propagate with constant speed c, we rewrite these solutions in a comoving reference frame as a function of a single space-time variable $\xi = x - ct$:

$$(u_p(x,t), v_p(x,t)) = (u_p(\xi = x - ct), v_p(\xi = x - ct)). \tag{11}$$

Rewriting Eqs. (1) for stationary solutions in the moving reference frame, we obtain a moving spatial dynamical system (MSDS):[1]

$$du/d\xi = y, \quad dv/d\xi = z, \quad dy/d\xi = -v - c\,y,$$
$$dz/d\xi = u^3 - \mu_2 u - \mu_1 - v(v + bu - u^2) - c\,z. \tag{12}$$

Nontrivial bounded trajectories of this system define the spatial shape of structures that propagate without changing shape with velocity c in the spatially extended system (1) [e.g., limit cycles of (12) describe traveling-wave solutions, homoclinic connections describe traveling pulses, and heteroclinic connections describe propagating fronts between homogeneous solutions].

We would like to point out some considerations about the MSDS. First, the MSDS gives straightforward information about the existence and shape of steady solutions of the PDEs in a moving reference frame. It does not provide information about the existence of other kinds of dynamical attractors, such as breathers or turbulent regimes.

Second, the MSDS has one more parameter than the PDEs, the velocity c. The PDEs can show, for a fixed parameter configuration, all the structures of the MSDS for any value of c. Therefore, the codimension of regions of existence of any structure is greater by a unit in the MSDS. For example, structures existing only on codimension-one bifurcations of the MSDS, as traveling pulses, will be codimension-zero in the PDEs.

As a consequence of the spatial reversibility (and time translation) of (1), the MSDS remains invariant under the involution:

$$R : (\xi, u, v, y, z, c) \to (-\xi, u, v, -y, -z, -c), \tag{13}$$

and, therefore, space reversed traveling solution will propagate with opposite velocity.

Fixed points of the system (12) describe the homogeneous solutions of the PDEs, i.e., the fixed points of the local dynamical system (2). Therefore, for simplicity, we will use the same notation for the fixed points of the local dynamical system and the MSDS. Linear stability analysis of these points, as well as local bifurcations of the MSDS system are discussed in Appendix B. It is important to notice that the MSDS (12) is not an excitable system in itself. This is because hypothetical excitations to its fixed points will, in general, not return to the same local stationary state, as should happen in a true excitable system. So, true features of excitability are observed in the local dynamics, not in the MSDS. Excitability manifests itself in the MSDS in the form of the homoclinic trajectories, which inherit properties of the temporal excitable excursions. These homoclinic connections are the excitable traveling pulses of the PDEs.

[1]The spatial dynamical systems in the moving reference frame is sometimes also referred to as traveling-wave ordinary differential equations (TWODEs) [30].

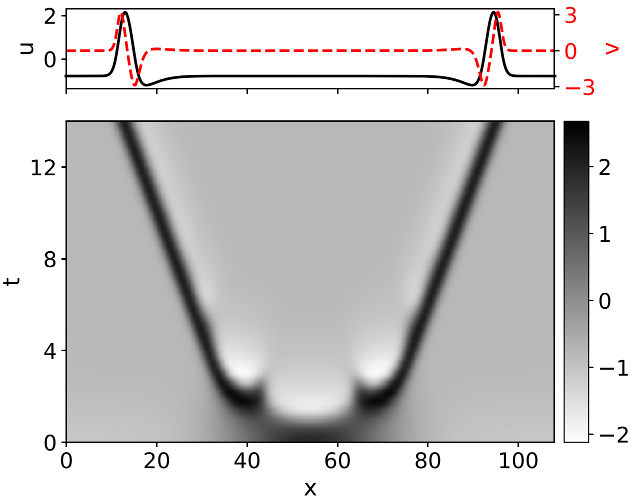

FIG. 3. Creation of a pair of traveling pulses from a Gaussian localized initial condition on top of the P_1 homogeneous solution. The main figure shows the spatiotemporal evolution of the u field for $\mu_1 = 0.3$ and $\mu_2 = 1.0$. The top panel shows the transverse profile of the u and v fields for $t = 14$.

There are two limit cases of special interest. The first case is the limit $c \to \infty$, which describes the temporal evolution of homogeneous solutions of the PDEs. Approaching this limit the evolution of bounded trajectories asymptotically slow down, while they approach the plane $(u, v, y, z : y = z = 0)$. Nevertheless, the time evolution of each point of the associated PDE solution ($\mathbf{u_t} = c\mathbf{u}_\xi$), converges to the local evolution of that point given by (1).

The second case is $c = 0$, which defines the steady solutions of the PDEs. In this particular case there is a set of points invariant under R, given by the plane $\Pi = (u, v, y, z : y = z = 0)$. Trajectories that cross Π are reversible and, therefore, achiral [31,32].

III. TRAVELING PULSE STABILITY REGION

A strong enough localized perturbation of the P_1 homogeneous solutions generates, for the appropriate parameter values inside the excitable region, a pair of traveling pulses that propagate in opposite directions in the media (Fig. 3). These pulses propagate without changing shape. Two such pulses also cancel each other when colliding. They are, therefore, excitable traveling pulses. In this paper we will refer to these traveling pulses with the P_1 solution as background state as TPs.

In the MSDS, a TP corresponds to a tangential homoclinic connection to the P_1 fixed point. This connection is created at a homoclinic bifurcation, in which limit cycles of the MSDS (waves trains of the PDEs) are destroyed. This bifurcation is codimension-one in the MSDS. As a consequence the TPs are isolated and their shape and velocity are independent of the

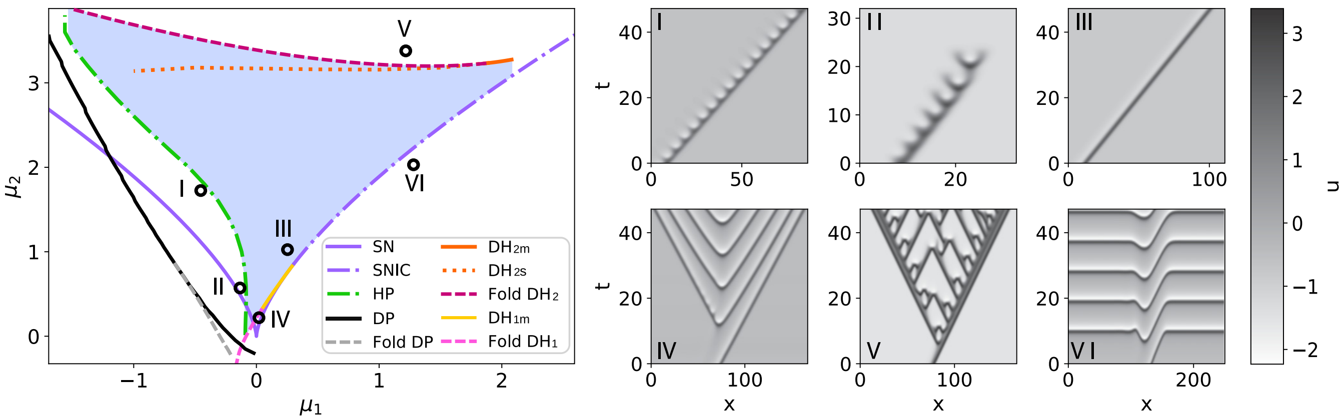

FIG. 4. Stability region of TP (shaded in blue). The stability region of the pulse is bounded by two monotonic double heteroclinic (DH) point bifurcation, DH_{1m} and DH_{2m} (light and dark orange solid lines), two folds associated with the DH_1 and DH_2 bifurcations (pink and magenta dashed lines), Hopf bifurcation of the pulse (HP) (green dashed dotted line) and the SNIC (purple dashed dotted line). Also have drew the drift pitchfork (DP) bifurcation line where the pulses are generated (black line), the fold associate with the DP (gray dashed line), the DH_2 with collapse snaking bifurcation (DH_{2s}, dark orange dotted line) and the SN bifurcation of the homogeneous solutions as a referential frame (purple lines). Insets (I)–(VI) show the dynamics observed for the different parameter values indicated in the main figure. (I) Stable oscillatory traveling pulse found once crossed the Hopf bifurcation (Sec. III A) of TP for $\mu_1 = -0.112$, $\mu_2 = 0.206$. (II). Propagation failure found once crossing the Hopf (Sec. III A) of pulses for $\mu_1 = -0.36$ and $\mu_2 = 1.46$. (III). Stable TP found in the shaded in blue region, for $\mu_1 = 0.3$, $\mu_2 = 1$. (IV). Time evolution of a pulse replication for $\mu_1 = 0$ and $\mu_2 = 0.21$, beyond the heteroclinic bifurcation I (Sec. III C). (V). Time evolution of the system in the turbulent regime found beyond the heteroclinic bifurcation II (Sec. III D) for $\mu_1 = 1.29$ to $\mu_2 = 3.21$. (VI). Time evolution of a pulse on top of the homogeneous oscillatory state for $\mu_1 = 1.9$ and $\mu_2 = 2.5$ found beyond the SNIC bifurcation (Sec. III B).

initial conditions in the PDE, thus shape and velocity depend exclusively on the choice of parameters.

The TP solution is a stable attractor in a part of the temporal excitable region. This stable part is shown in blue in Fig. 4 and is limited by four different bifurcations: a Hopf bifurcation of TPs (HP, dot-dashed green line) on the left, a SNIC bifurcation (dot-dashed purple line), a double heteroclinic bifurcation (DH_{1m}, solid light-orange line), and a fold of TPs (fold DH_1, dashed pink line) on the right, and by a double heteroclinic bifurcation (DH_{2m}, solid dark orange line) and a fold (fold DH_2, dashed magenta line) on the top. In the following sections we discuss each one of these bifurcation lines and the regimes arising when each threshold is crossed. The SNIC and double heteroclinic bifurcation (DH_{1m}) were already studied in Ref. [28].

A. Hopf bifurcation of traveling pulses

On the left, the stable region is limited by a Hopf bifurcation of the TP (green dot-dashed line in Fig. 4). A linear stability analysis of the TP solution of (1) reveals that, at this bifurcation, a pair of complex-conjugate eigenvalues cross the imaginary axis, destabilizing the TP in an oscillatory manner. The corresponding eigenfunction is localized and has its maximum modulus at the back of the pulse.

Numerical simulations of a TP for parameters beyond this bifurcation show that for values of μ_2 in the lower part of Fig. 4 the Hopf is supercritical and the system tends to a stable breathing traveling pulse-like solution like the one shown in Fig. 4(I). This pulse propagates while presenting low amplitude periodic oscillation of its width and amplitude, specially on the back of the pulse. The amplitude of the oscillations increases as the parameters are moved away from Hopf bifurcation. These results are similar to those shown in Ref. [30]. For larger values of μ_2 the Hopf is subcritical and initial conditions close to the unstable TP end up in failure of propagation, as shown on Fig. 4(II). The TP initially shows some oscillations, but after propagating for some time its amplitude decreases until vanishing eventually, decaying to the rest state.

B. Saddle-node on the invariant cycle bifurcation

The stability region of TPs is limited on the right by the SNIC bifurcation (dot-dashed purple line). The TP exists all the way until the SNIC line, experiencing a divergence of its width as the parameters approach the SNIC [28]. More details of such bifurcation are given in Sec. IV A. After crossing the SNIC bifurcation line in parameter space the P_1 homogeneous steady solution disappears when colliding with the P_2 fixed point in a saddle-node, leading to a homogeneous oscillation. A TP-like initial condition for these parameter values forms a pulse on top of the homogeneous oscillation [see Fig. 4(VI)]. As the background oscillates, the localized structure corresponding to a TP before the bifurcation is now reset at each oscillation. After propagating briefly, the background oscillation brings the localized structure back to the initial position. The system shows then an almost periodic behavior, as can be seen in Fig. 4(VI). For some of the simulations we did for different parameter values we observed a drift in the position of the localized structure after each oscillation of the ground state. This drift is much slower than the velocity of the localized structure during the oscillation.

C. Double heteroclinic bifurcation I

On the lower right part of the stable region the SNIC line terminates at a saddle-node separatrix-loop (SNSL) codimension-two point and the stability region is from there on delimited by a monotonic double heteroclinic bifurcation line DH_{1m}, starting from the same point, and a fold of TPs (fold DH_1). The double heteroclinic bifurcation is explained in more detail in Sec. IV B. Past these bifurcations, a pulse develops a protuberance in its tail that will eventually generate two pulses propagating in opposite directions [see Fig. 4(IV)]. This process repeats generating two wave trains propagating in opposite directions, and it is known in the literature as "backfiring" [33].

D. Double heteroclinic bifurcation II

At the upper part, the stability region is delimited by a monotonic double heteroclinic bifurcation and a fold of TPs, labeled DH_{2m} and fold DH_2 in Fig. 4. A detail description of the scenario leading to such bifurcations is given in Sec. IV B. An initial pulse for parameter values past the DH_2 bifurcation starts losing its shape and, after some time, the tail of the pulse grows a perturbation which eventually travels as a pulse in the opposite direction. Both pulses start generating new pulses that annihilate when colliding and, sometimes, generate even more pulses. This process generates a spatiotemporal chaotic regime that propagates until taking up all the system. An example of such dynamics is shown in Fig. 4(V), which resembles spatiotemporal intermittency [34]. This turbulent regime is also related to the phenomenon of backfiring [33].

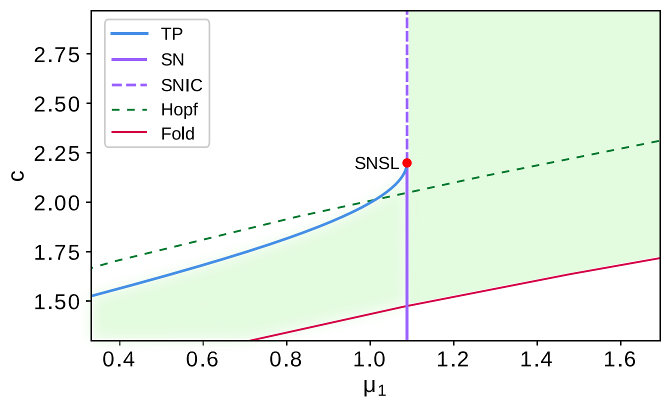

FIG. 5. Phase diagram of the MSDS for $\mu_2 = 2$, close to the SNIC bifurcation of the temporal system (indicated by the vertical purple line). The blue line is the homoclinic bifurcation whose associated homoclinic trajectory corresponds to a TP. This bifurcation line ends at a codimension-two point (SNSL) when colliding with the SN bifurcation of the homogeneous solutions (purple line). The SNSL indicates the end of the existence of TPs in correspondence with the SNIC of the homogeneous solutions. The green shaded region indicates the existence of limit cycles in the MSDS, i.e., wave trains on the PDEs, whose period diverge at the SNIC and homoclinic bifurcations. The dashed green and red lines indicate, for completeness, a Hopf bifurcation of P_3 and a fold of cycles where such wave trains are created or destroyed.

IV. MOVING SPATIAL DYNAMICAL SYSTEM BIFURCATIONS

In this section we analyze in detail some of the bifurcations discussed above from the point of view of the moving spatial dynamical system (MSDS).

In the PDEs (1), TPs are codimension-zero, i.e., they exist for any parameter values within the existence region, where their velocity is uniquely determined by the parameters. However, in the MSDS (12), where the velocity c of the moving reference frame is a free parameter, TPs are codimension-one, i.e., once the other parameters are fixed, they only exist for the precise value of c corresponding to the velocity of the TP in the PDEs. As a TP corresponds to a homoclinic trajectory in the MSDS, this value of c indicates the exact location of a homoclinic bifurcation in the (μ, c) parameter space. For the parameters values where P_1 is a saddle bifocus (see Appendix B) the homoclinic bifurcation shows Shilnikov characteristics [35]. This implies the existence complex limit cycles in the MSDS, which describe spatially chaotic traveling structures. The Shilnikov's effect and the presence of these structures do not affect the results presented in this work.

A. Saddle-node on invariant cycle as a saddle-node separatrix-loop in the moving spatial dynamical system

The SNIC bifurcation of the temporal system is somehow more complicated in the MSDS. In the MSDS the SN and the homoclinic bifurcations associated with the TPs are codimension-one. The bifurcation where the TPs are destroyed is described by a codimension-two bifurcation where these two manifolds meet. The full unfolding of this bifurcation point is shown on Fig. 5. The SN of the MSDS occurs for the value of μ_1 corresponding to the SNIC bifurcation of the temporal system, and is indicated by the vertical purple line in Fig. 5. To the left of this line, TPs correspond exactly to the homoclinic trajectory created at the homoclinic bifurcation (blue line in Fig. 5). To the right they do not exist as explained in Sec. III B. Then, following the homoclinic bifurcation line, we observe that TPs terminate at the precise value of μ_1 where the homoclinic bifurcation line (in blue) touches tangentially the SN bifurcation (purple vertical line). This codimension-two point corresponds to a SNSL in the MSDS, marked as a red point on Fig. 5. Therefore, the SNIC bifurcation of a TP is always a SNSL in the MSDS. Notice that, close enough to the SNSL, the eigenvalues of P_1 are real (see Appendix B) and the homoclinic bifurcation associated with the TP does not show Shilnikov's effect.

This SNSL separates two different cases of the SN bifurcation where P_1 and P_2 collide. For velocities c above the SNSL point, the SN is a saddle node on the invariant cycle bifurcation (SNIC, dashed purple line). The invariant cycle on where the homogeneous solutions appear describes (not necessarily temporally stable) wave trains, shown in Fig. 5 as the shaded green region. The period of these large velocity wave trains diverge as the parameters approach the SNIC bifurcation from the right, and, therefore, do not coexist with the TP. For velocities below the SNSL, the SN of the homogeneous solutions corresponds to a saddle node off the invariant cycle (solid purple line) and, therefore, slow wave trains (not necessarily temporally stable) expand inside the excitability region all the way to the homoclinic bifurcation (blue line), where their period also diverges. The origin of these wave trains on the MSDS can be linked to a Hopf and a

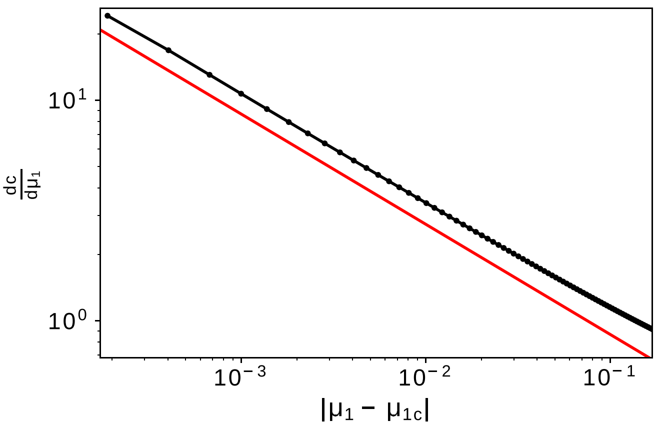

FIG. 6. Scaling of the derivative of the velocity of the TP with respect to μ_1 in the proximity of the SNSL. The expected theoretical scaling is shown in red for comparison.

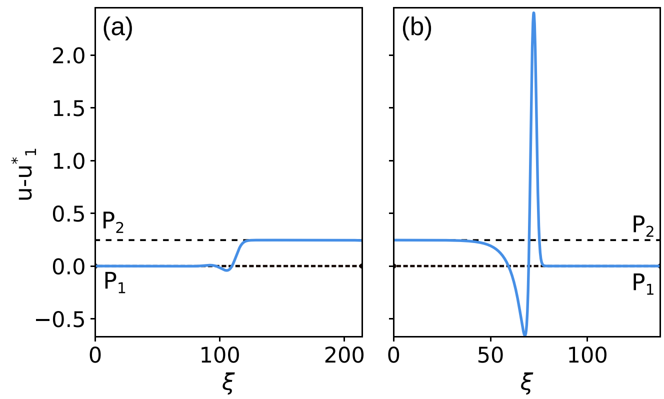

FIG. 7. The two heteroclinic connections (fronts in the PDE) between P_1 and P_2 on the DH_{2m} point for $\mu_1 = 0.4$. (a) Back-heteroclinic connection (h_b). h_b is part of a parametrized by velocity family of fronts of P_1 into P_2, its velocity is selected by the velocity of h_f. (b) Front-heteroclinic connection (h_f).

fold of cycles shown in dashed green and red lines in Fig. 5, respectively. These bifurcations are not relevant for the main discussion of this work and are only shown for completeness.

The proximity to the SNSL bifurcation affects the TP in two different ways. First, it slows down the approach to the rest state, being on the SNSL slower than exponential. This effect was studied in detail in Ref. [28] and is associated with the tendency of the slow eigenvalue of P_1 when approaching the SN. Second, the derivative of the pulse velocity, which is the value of c of the homoclinic bifurcation, with respect to the control parameter (μ_1) diverges when approaching the bifurcation as $dc/d\mu_1 \propto 1/\sqrt{\mu_1}$. This scaling is shown in Fig. 6.

B. Double heteroclinic bifurcations I and II

The double heteroclinic bifurcations I and II described in Secs. III C and III D are associated with double heteroclinic connections between P_1 and P_2 in the MSDS, where each heteroclinic describes a different propagating front in the PDEs [36]. The first of these heteroclines, which we name back-heteroclinic connection (h_b), is given by a transverse intersection of the two-dimensional unstable manifold of P_1 and the three-dimensional stable manifold of P_2. The h_b is then a codimension-zero solution of the MSDS. This implies the existence of a continuous family of propagating fronts of P_1 into P_2 for parameter values in the neighborhood of the bifurcation point, which are characterized by their velocity. An example of this front is shown on Fig. 7(a).

The other heteroclinic connection, which we name front-heteroclinic connection (h_f), is given by the tangential intersection of the one-dimensional unstable manifold of P_2 and the two-dimensional stable manifold of P_1. This connection is codimension-two in the MSDS, which implies that the propagating front of P_2 into P_1 is not generic and exists only at the bifurcation. An example of this front is shown in Fig. 7(b). From the interaction between these two fronts emerges the homoclinic connection corresponding to the TP.

This double heteroclinic (DH) bifurcation is known in the literature as T-point [37]. Close to the DH point, we can interpret the emerging traveling pulse as the pinning of two weakly interacting fronts, with h_b chasing h_f separated by a large plateau close to P_2. The plateau width will diverge to infinite while approaching the DH point.

From the DH point, another homoclinic connection emerges, in this case bi-asymptotic to the P_2 solution, associated with an unstable traveling pulse on top of the P_2 homogeneous solution. Similar to the traveling pulse on P_1, these pulses will generate a plateau, in this case around P_1 as the parameters approach the DH point. Close to the bifurcation these traveling pulses can be interpreted as two weakly interacting fronts, in this case with h_f chasing h_b, separated by a large plateau close to P_1. This plateau diverges to infinite as the parameters approach the DH point. We refer to these traveling pulses with P_2 as background as TP_2.

Strictly speaking, the DH point exists only for infinite-domain systems. In finite systems with periodic boundary conditions we find, instead, a transition from the TP with P_1 background to the traveling pulse with P_2 background (TP_2). This transition occurs in one (or more [30]) folds of the traveling pulses close to the region in the parameter space where the DH point is found in the infinite-domain system.

The weak interaction between fronts is given by the overlap of their asymptotic decay to P_2 [38,39]. This decay is determined by the spatial eigenvalues of P_2. Two different scenarios can be found on this DH point depending on how h_b tends asymptotically to P_2:

1. Monotonic double heteroclinic point

We first discuss the case when h_b tends to P_2 monotonically, i.e., when the stable spatial eigenvalues of P_2 are real at the DH point. In this case, the interaction between a h_b and a h_f fronts separated by a plateau on P_2 decreases monotonically with the distance between the fronts [38]. As a consequence, the TP branch approaches the DH point also monotonically, without snaking (Fig. 8).

As mentioned above, when approaching the DH point the TP starts to present a plateau around P_2 (see the inset of Fig. 8). The plateau width diverges logarithmically with the distance of the control parameter to the DH point [28].

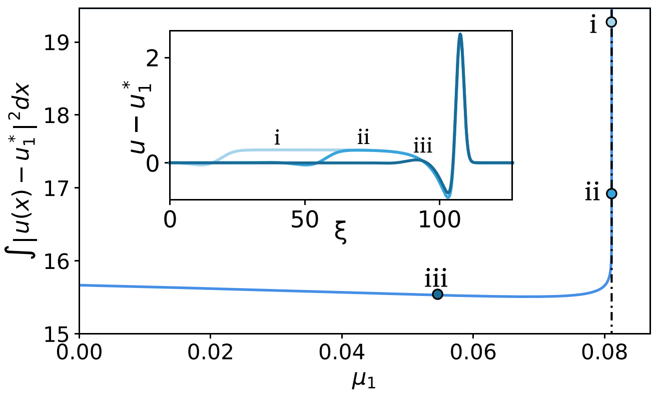

FIG. 8. Bifurcation diagram of the TP solution close to the DH_1 point for $\mu_2 = 0.4$ (marked with a vertical dashed dotted line). The width of the TP, as measured by the norm of the TP, diverges monotonically at the bifurcation. Inset shows the profile of the TP for the three different values of μ_1 indicated in the main figure.

Close to the DH point, where the TP has an arbitrarily long plateau tending to the unstable homogeneous solution P_2, one could expect the TP to be unstable, but, actually, in this case the plateau is only convectively unstable in the comoving reference frame, being the TP globally stable. The other case, where the plateau is absolutely unstable, corresponds to the collapsed snaking case we will discuss below [30,36,40]. Close enough to SN_{r-}, the DH point is always monotonic.

2. Collapsed snaking

In this section, we consider the case when the asymptotic tendency of h_b to P_2 is oscillatory, i.e., when P_2 has complex eigenvalues at the DH point. In this case, the interaction between h_b and h_f changes periodically from attractive to repulsive with the distance between them, while the interaction strength decays exponentially, allowing two fronts to lock (or pin) at discrete separation lengths. This causes the homoclinic bifurcation curve corresponding to the TP to snake towards the DH point (Fig. 9). From the PDE point of view, the TP has to turn infinitely many folds while the parameters approach the DH point. At each fold, the width of the pulse increases in half the wavelength of the asymptotic oscillations of the front h_b profile. As a result of the fronts locking, at the DH point there are infinitely many TPs with different widths. The envelope of the bifurcation line shows a characteristic divergence as a function of the distance to the DH point as in the previous case. This phenomenon is known as collapsed snaking [41]. In this case, the TP loses its stability when the plateau starts to form after the first fold, and at each successive fold it gets an extra positive eigenvalue [Fig. 9(e)] [30]. This is different from the usual collapsed snaking, where the stability changes at each fold, the reason being that, in this case, the homogeneous state of the plateau is absolutely unstable.

The approach of the TP_2 to the DH point presents both same scenarios as the TP. Monotonic or oscillatory is determined in this case by the eigenvalues of P_1 at the DH point. The approach is monotonic if the eigenvalues of P_1 are real, and snaking is observed otherwise. In particular, the approach is monotonic close enough to SN_{r-}.

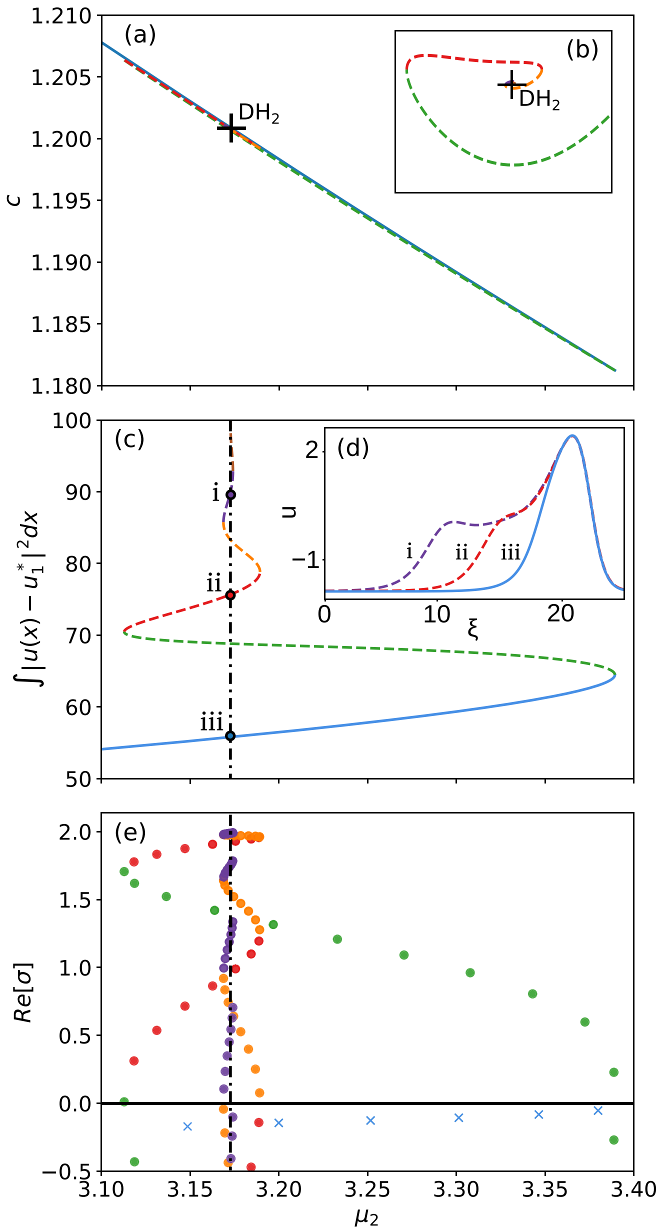

FIG. 9. (a) Phase diagram of the MSDS in the (c, μ_2) parameter space for $\mu_1 = 0$ and around the DH_2 bifurcation point (indicated by a black cross). The panel can also be interpreted as a bifurcation diagram of the PDEs where the curves represent different branches of TPs, spiraling around DH_2. The axis orientation makes difficult to differentiate the different lines, so in panel (b) we have stretched the parameter space around DH_2 to better show the spiraling of the bifurcation lines. The axis of this inset are no longer μ_2 and c, but a linear combination of them. (c) Bifurcation diagram of the TP solution close to the DH_2 point in the collapsed snaking case for $\mu_1 = 0$. Solid (dashed) lines indicate stable (unstable) solutions. The value of μ_2 corresponding to the DH_2 point is marked with a vertical dashed dotted black line. (d) Spatial profiles of the field $u(\xi)$ for the different branches indicated in the main figure. (e) Real part of the most unstable eigenvalues of the TP as function of the parameter μ_2. Dots represent real eigenvalues and crosses complex-conjugate pairs. The color indicates the corresponding branch of the TP. Translationally invariant zero eigenvalues have been omitted.

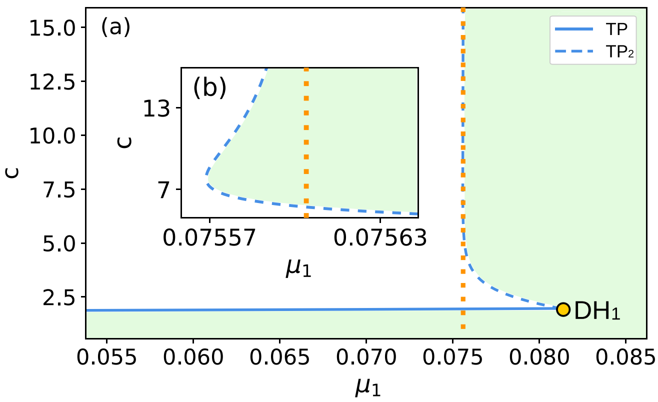

FIG. 10. (a) Bifurcation diagram around the DH_1 bifurcation point for $\mu_2 = 0.4$. The homoclinic bifurcations creating the TP (solid blue) and TP_2 (dashed blue) converge at the DH point. The velocity of the TP_2 has an asymptotic divergence when approaching the temporal homoclinic bifurcation point (L_-^b), indicated by the vertical dotted orange line. At this point and in the $c \to \infty$ limit the TP_2 converges to the homogeneous temporal homoclinic connection. (b) Detail of TP_2 close the parameter value of L_-^b.

The transition between both scenarios is given by a codimension-three point (codimension-two in the PDEs parameter space) given by the transverse intersection between the DH bifurcation codimension-two manifold and a Belyakov-Devaney pseudobifurcation codimension-one manifold, (see Appendix B). At this codimension-two point, the double heteroclinic connection occurs while the P_2 point have an algebraically degenerate real eigenvalue. The Belyakov-Devaney pseudobifurcation indicates, precisely, the drift speed at which the P_2 homogeneous solution changes from being convectively unstable to being absolutely unstable. Further information about convective and absolute instabilities can be found in Refs. [36,42].

C. Connection between temporal and spatio-temporal bifurcations of traveling pulses

In this section, we discuss the connection between the (spatial) bifurcations of the MSDS and the (temporal) bifurcations of the local dynamics. We focus on the homoclinic bifurcation associated with the TP_2 in the limit $c \to \infty$. In this limit, as already mentioned in Sec. II B, the MSDS recovers the temporal equations. In particular the TP_2 emerges from the temporal homoclinic bifurcation for $c = \infty$ and becomes a stable excitable TP at the DH_1 point for a finite velocity.

The homoclinic connection that forms at the homoclinic bifurcation unfolding from DH_1 (DH_2) (dashed line in Fig. 10) corresponds to TP_2. We observe how, when the parameters approach the values associated with the homoclinic temporal bifurcation L_-^b (L_-^s), (dotted vertical line) the velocity of the TP_2 diverges to infinity. At the same time, the dynamics of the MSDS slows down making the pulse wider. These two asymptotic behaviors show the tendency of the solution of the MSDS in the limit $c \to \infty$, where the local dynamics of the system are recovered. Therefore, the homoclinic connection that TP_2 represents in the MSDS tends in this limit to the temporal homoclinic connection of the local dynamics of the system on L_-^b (L_-^s).

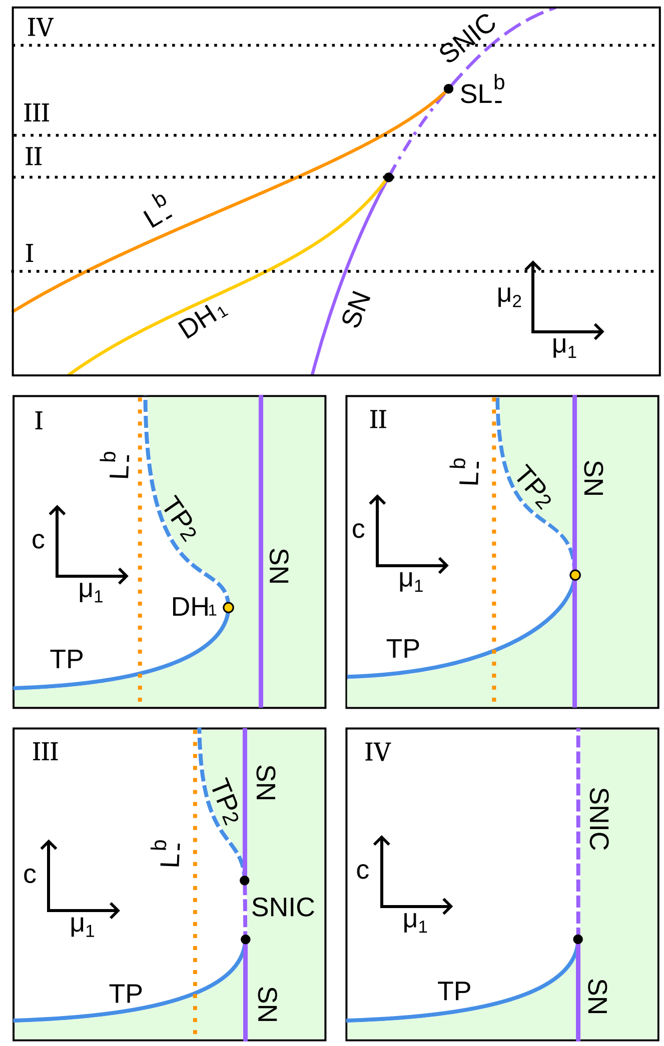

FIG. 11. Schematic phase diagram around the $SNSL_-^b$ which shows the tangential point between the temporal bifurcation line L_-^b and the SN_r; and the spatiotemporal bifurcation DH_1 and the SN_r. In the four small down panels are shown bifurcation diagram of the PDEs (related with phase diagrams of the MSDS) for the four different fixed μ_2 lines shown in the phase diagram. On this bifurcation diagram the solid blue lines represent the TP with rest point on P_1, the dashed blue lines represent the unstable TP with rest state on P_2, the purple line represent the SN bifurcation on the MSDS and the orange line shown the μ_1 value where the L_-^b occurs in the temporal model. Green colored region of the bifurcation diagrams represent traveling waves (oscillatory region of the MSDS).

This connection between the TP_2 and the homoclinic trajectory of the temporal system establishes a bridge between the temporal excitable trajectory and the traveling pulses [28].

Furthermore, the connection between DH_1 and L_-^b allows us to understand the transition between DH_1 and SNSL of TPs bifurcations. This transition is illustrated in Fig. 11, where different cuts of the parameter space of the PDEs are shown. Figures 11(I) to 11(IV), corresponding to the four different cuts of the main figure indicated by the horizontal dotted lines, can be interpreted as bifurcation diagrams of the PDEs or phase diagrams of the MSDS.

Close enough to the SN_{r-} bifurcation point both, P_1 and P_2, have real eigenvalues and therefore the approach of the TP and the TP_2 to the DH_1 point is monotonic. This is illustrated in a first cut of the parameter space, where the DH bifurcation occurs between the L^b_- and the SN [Fig. 11(I)]. Notice the similarities between this schematic representation and the numerical result shown in Fig. 10.

The DH point approaches the SN when increasing μ_2 until it tangentially touches the SN_r bifurcation. At this codimension-two point of the PDEs (codimension-three in the MSDS) the system presents a homoclinic connection of a nonhyperbolic point. A bifurcation diagram cutting through this high-codimension point is shown in Fig. 11(II).

Beyond this point the TP and TP_2 branches are separated, ending each one at the SN in a SNSL of the MSDS. The SN bifurcation between these two SNSL is a SNIC of the MSDS. This case is illustrated in Fig. 11(III).

Eventually, the L^b_- bifurcation touches the SN_r bifurcation, corresponding to the SNSL of the temporal system. Beyond this point the TP_2 does not exist anymore, while the TP still ends in a SNSL bifurcation of the MSDS. This case corresponds to the one described in Sec. IV A. A schematic phase diagram of this scenario is illustrated in Fig. 11(IV). Notice the similarities between this scheme and the numerical result shown on Fig. 5.

Other bifurcations of the temporal system percolate in the MSDS through the limit $c \to \infty$. This is the case of the temporal Hopf bifurcation and fold of cycles, which in the MSDS generate the cycles (waves trains in the PDEs). Higher codimension points involving these bifurcations, such as degenerate loops points, could affect the stability of the pulses. These bifurcations have not been observed for the considered parameter values. Nevertheless, it is expected that for other values of the parameters these bifurcations will have an effect on the stability of the pulses.

V. DRIFT PITCHFORK

The existence of TPs can be tracked down to the SN_r for $c = 0$, in particular for the same parameters of SN_{r-} in the temporal case. For $c = 0$ the fixed points belong to the symmetry plane Π and therefore the linearization around them is strongly symmetric. In particular the eigenvalue problem on SN_{r-} is degenerate, having the degenerate fixed point two opposite real and two nondiagonalizable zero eigenvalues. This point is known as reversible Takens-Bogdanov (RTB).

A small amplitude homoclinic reversible connection of the fixed point P_1 is part of the unfolding around the RTB [43,44]. This homoclinic connection is translated into low-amplitude achiral steady localized structures (LS) of the PDEs. This LS is unstable, and its amplitude grows decreasing μ_1 away from the RTB until it reaches a fold (Fig. 12). After the fold, it keeps growing in amplitude, but now increasing μ_1, until it reaches a second fold. After this second fold the LS starts changing its shape: the middle point of the pulse starts developing a local minimum for both (u, v) fields and the pulse starts decreasing in amplitude. After a third fold, while it reaches out again to the RTB, the pulse decreases in amplitude while the local

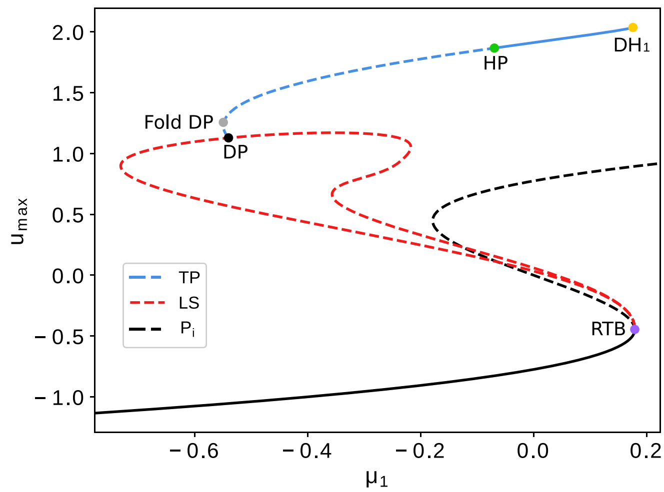

FIG. 12. Bifurcation diagram of LS and TP solutions for $\mu_2 = 0.6$. The diagram shows the maximum value of u (u_{max}) of the different solutions as function of μ_1. Solid (dashed) lines represent stable (unstable) solutions. The black line represents the homogeneous solutions, the red line the LS, and the blue line the TP. The LS branch starts from the right SN (SN_r, RTB) represented by a purple dot. The TP branch starts at the nonequilibrium Ising-Bloch transition, also known and drift-pitchfork (DP) shown as a black dot, followed by its associated fold of pulses showed as a gray dot. The TP changes its stability at the Hopf bifurcation (HP) (green dot) and ends at the DH_1 bifurcation (light orange dot).

minimum in the middle of the pulse approaches P_1, effectively splitting the LS in two. This approach to the fixed point comes with a slowing down in the ξ dynamics and, close enough to the RTB, the two small-amplitude peaks separate half of the system size. From this endpoint starts a new branch of LS very similar to the previously discussed one, but with two LSs separated half the system size. Similar behavior has been found in other systems [45,46].

TPs are generated from this LS at a nonequilibrium Ising-Bloch transition, also known as drift-pitchfork bifurcation (DP), between the first and second folds of the LS [47–49]. The emerging TP breaks the chiral symmetry of the LS and propagates in space with nonzero velocity c. The chiral forks of the pitchfork represent the two mirror-image TP propagating in opposite directions. Some vegetation models show a similar mechanism for the creation of traveling pulses outside the excitable region [50,51].

The DP bifurcation changes from supercritical to subcritical on a degenerate codimension-two point. A fold of traveling pulses is part of the unfolding of this high codimension point. This fold is shown as a gray line on Fig. 4 and as a gray dot in Fig. 12.

VI. CONCLUSION

We have studied the mechanisms behind the creation (or destruction) of traveling pulses in a general model for type-I excitable media. Traveling pulses are stable only in part of the excitable region of the local dynamics. They destabilize through different transitions related with the bifurcations of the local dynamics delimiting the excitable region in the parameter space but can also undergo purely spatiotemporal instabilities. The latter, referring to Hopf bifurcation of the TP, is a secondary bifurcation of the TP leading to the destabilization of the pulses and, in some cases, the creation of other propagating localized structures [see Figs. 4(I) and 4(II)]. The former, which are those that give rise to TP, i.e., the saddle-node separatrix-loop and the double heteroclinic (T-point), have been studied in a comoving spatial dynamics description (moving spatial dynamical system, MSDS), which has been shown to converge to the temporal dynamics in the limit in which the speed is very large. Exploiting this limit we have been able to connect these bifurcations of the traveling pulses to the temporal bifurcations leading to type-I excitability, i.e., the SNIC and homoclinic bifurcations. Beyond this connection, we have also shown that traveling pulses bifurcate from generic steady localized structures in bistable systems through a drift pitchfork bifurcation.

The connection between spatiotemporal and pure temporal bifurcations is general and gives some insight in the properties of traveling pulses in type-I excitable media as compared with those in type-II. The distinction between these two cases is not a simple academic exercise but has important implications when trying to model excitable behavior found in natural systems. Often the straightforward approach is using variants of a textbook model: the FitzHugh-Nagumo equation [2], which is a paradigm for type-II excitability. Instead, many models based on biological mechanisms and general principles put forward in recent years show signs of type-I excitability, as they exhibit homoclinic phenomena, well-defined thresholds, and the resultant signature on the (unbounded) periods of excitations [20–24]. The consequence is that the observed excitable behavior might not correspond to the characteristic behavior of a type-II excitable medium but, instead, may correspond to a type-I excitable medium. In this work and the companion paper [28] we have analyzed in detail pulses that propagate in type-I excitable media, and their main features. We hope this will appeal to experimentalists that might be observing these novel manifestations of excitable dynamics.

Our study has described TP in an excitability scenario where the fixed points emerge from two saddle-node bifurcations organized by a cusp codimension-two point. Nevertheless, some vegetation models present a variant of our route to type-I excitable behavior based on a transcritical bifurcation, due to the constraint that populations cannot become negative [21–23]. Therefore, a natural extension of our work is to study in detail the scenario in which a transcritical bifurcation instead of a saddle-node organizes the system in parameter space. Also, in a model defined on a one-dimensional spatial domain, as used in the present work, it is not possible to study spatiotemporal structures like rings or spirals, that have been observed experimentally [21,22], and a logical extension is to study the scenario in a two-dimensional system.

ACKNOWLEDGMENTS

We acknowledge financial support through grants RTI2018-095441-B-C22 and MDM-2017-0711 funded by MCIN/AEI/10.13039/501100011033 and by ERDF A way of making Europe. D.R-R. is supported by the Ministry of Universities through the "Pla de Recuperació, Transformació i Resilència" and by the EU (NextGenerationEU), together with the Universitat de les Illes Balears. A.A-i-P. is financed by Czech Science Foundation, Project No. GA19-16066S.

APPENDIX A: GLOSSARY OF FREQUENTLY USED ACRONYMS AND SYMBOLS

P_i: Homogeneous steady solutions of Eq. (1).

TP: Traveling pulse on P_1.

TP_2: Traveling pulse on P_2.

SNIC: Saddle-node on invariant cycle.

PDEs: Partial differential equation system. Usually refers to the one given by Eq. (1).

SN_l (SN_r): Left (right) branch of saddle-node bifurcation. Bifurcation of the local dynamical system.

$\lambda_\pm$: Eigenvalues of the local dynamical system's fixed points [Eq. (2)].

H_1 (H_2): Andronov-Hopf bifurcation of the fixed point P_1 (P_2). Bifurcation of the local dynamical system.

B: Bautin point, a.k.a. degenerate Hopf. Bifurcation of the local dynamical system.

DL^b (DL^s): Big (small) degenerate saddle-loop point. Bifurcation of the local dynamical system.

L_+^b or L_-^b (L_+^s or L_-^s): Big (small) saddle-loop (a.k.a. homoclinic) bifurcation with positive or negative saddle index, respectively. Bifurcation of the local dynamical system.

TB_l (TB_r): Takens-Bogdanov bifurcation point located on the left (right) branch of the saddle-nodes bifurcation. Bifurcation of the local dynamical system.

MSDS: Moving spatial dynamical system, given by Eq. (12).

R: Space reflection involution given by Eq. (13). Symmetry of the MSDS.

Π: Invariant plane under involution R.

HP: Andronov-Hopf bifurcation of TPs. Bifurcation of the PDEs.

DH_m (DH_s): Double monotonic (snaking) heteroclinic bifurcation, a.k.a. T-point. Bifurcation of the MSDS.

DP: Drift pitchfork bifurcation of pulses. Bifurcation of the PDEs.

SNSL: Saddle-node separatrix-loop of the MSDS system. Bifurcation of the MSDS.

RTB: Reversible Takens-Bogdanov bifurcation. Bifurcation of the MSDS.

APPENDIX B: FIXED POINTS AND LOCAL BIFURCATIONS AT THE MOVING SPATIAL DYNAMICAL SYSTEM

In this Appendix we study the linear dynamics around the fixed points of the MSDS. This provides the local bifurcation of the MSDS as well as the behavior of the trajectories close to the fixed points. Since the pulses and localized structures are described as homoclinics of a fixed point, the linear regime determines the shape of their tail as well as being involved in the creation and bifurcations of these structures.

Linearization of Eq. (12) around the fixed points is determined by four spatial eigenvalues given by

$$\lambda'_j(P_i) = \lambda'_j(u_i^*) = \frac{-c \pm \sqrt{c^2 - 4\lambda_\pm(u_i^*)}}{2}, \quad j = 0, 1, 2, 3, \tag{B1}$$

where $\lambda_\pm(u_i^*)$ are the temporal eigenvalues of the fixed point given by Eq. (5).

First, we present the codimension-zero eigenvalues configuration of the different fixed points for $c > 0$ and the codimension-one transitions between them. Second, we present the codimension-one solutions for the steady state ($c = 0$), which gives the transition between positive and negative velocity regions, and the codimension-two transitions between them. Due to the symmetry under involution (13), opposite velocity will give sign-changed eigenvalues.

The point P_2 presents two different codimension-zero configuration depending on the velocity:

(i) $c^2 > 4\lambda_+$: Three real negative and a single positive eigenvalue (saddle).

(ii) $c^2 < 4\lambda_+$: Two complex-conjugate eigenvalues with negative real part, a negative real eigenvalue, and a positive eigenvalue (saddle-focus).

The transition between saddle and saddle-focus occurs in a Belyakov-Devaney (BD) pseudobifurcation when $c^2 = 4\lambda_+$. This point has a real negative eigenvalue and two positive eigenvalues, one of them degenerate.

Points P_0, P_1, and P_3 can present different eigenvalues configurations depending on the parameters and velocity:

(i) When $\tau(u_i^*) < 0$ and $4\Delta(u_i^*) < \tau^2(u_i^*)$ (P_i is a stable node in the temporal system) the fixed point presents four real eigenvalues, two of them positive and the other ones negatives (bisaddle).

(ii) When $\tau(u_i^*) < 0$ and $4\Delta(u_i^*) > \tau^2(u_i^*)$ (P_i is a stable focus in the temporal system) the fixed point presents two complex-conjugate eigenvalues with positive real part and two complex-conjugate eigenvalues with negatives real part (saddle bifocus).

(iii) When $\tau(u_i^*) > 0$ and $4\Delta(u_i^*) < \tau^2(u_i^*)$ (P_i is an unstable node in the temporal system) the fixed point presents, depending on the velocity and parameters, three different configurations of eigenvalues:

(a) $c^2 > 4\lambda_+$: Four real negative eigenvalues (node).

(b) $4\lambda_- < c^2 < 4\lambda_+$: Two real negative eigenvalues and two complex-conjugate eigenvalues with negative real part (focus-node).

(c) $c^2 < 4\lambda_-$: Four by pairs complex-conjugate eigenvalues with the same negative real part (aligned-bifocus).

(iv) When $\tau(u_i^*) > 0$ and $4\Delta(u_i^*) > \tau^2(u_i^*)$ (P_i is an unstable focus in the temporal system) the fixed point presents, depending on the velocity and parameters, two different configuration of eigenvalues:

(a) $c < \{[4\Delta(u_i^*) - \tau^2(u_i^*)]/[2\tau(u_i^*)]\}^{1/2}$: Two complex-conjugate eigenvalues with positive real part and two complex-conjugate eigenvalues with negatives real part (saddle-bifocus).

(b) $c > \{[4\Delta(u_i^*) - \tau^2(u_i^*)]/[2\tau(u_i^*)]\}^{1/2}$: Four by pairs complex-conjugate eigenvalues with negative real part (bifocus).

The transition from node to focus-node configuration occurs in a BD when $c^2 = 4\lambda_+$. At this transition, the fixed point presents three real negative eigenvalues, one of them degenerate. The transition from focus-node to aligned-bifocus occurs in a BD at $c^2 = 4\lambda_-$. At this transition the fixed points presents two complex-conjugate eigenvalues and a real eigenvalue, all of them with the same negative real part. The transition from aligned-bifocus to bifocus occurs through a degenerate bifocus where the fixed point has a pair of complex-conjugate degenerate eigenvalues. The transition from node to bifocus occurs in a double BD point where the eigenvalue configuration has a pair of degenerate real eigenvalues. The transition from bifocus to saddle-bifocus occurs thought a Hopf bifurcation where small amplitude traveling waves are created. Finally, the transition from saddle-bifocus to bisaddle occurs in a double BD transition, in this case one of the degenerate eigenvalues is negative while the other one is positive.

The points P_1 and P_3 are generated in saddle-node bifurcations involving P_2. At this codimension-one bifurcation, there are different eigenvalues compositions of the fixed point.

The fold involving a saddle and a bisaddle occurs through a saddle-node$_+$ with two negative real eigenvalues, a positive eigenvalue, and a zero eigenvalue. The fold involving a saddle and a node occurs through a saddle-node$_-$ with tree negative real eigenvalues and a zero eigenvalue. Finally, the fold involving a saddle-focus and a focus-node takes place through a focus-saddle-node$_-$ with a real negative eigenvalue, two complex-conjugate eigenvalues with negative real part and a zero eigenvalue.

Fixing $c = 0$ we arrived to the steady codimension-one configurations. Even if this region is codimension-one in the MSDS, as we are fixing the velocity, which is not a parameter of the PDEs but a condition for selected from the different traveling solutions, the steady solutions are relevant and codimension-zero in the PDEs. As the fixed points P_i belong to the symmetry plane Π the eigenvalues have a strong symmetry and can be seen as pairs of opposite complex numbers.

The point P_2 presents a single eigenvalue configuration when $c = 0$. Two of their eigenvalues are opposite real while the other two are opposite imaginary (center-saddle).

The points P_0, P_1, and P_3 can present three different configurations depending on the parameters:

(i) When $\tau(u_i^*) > 0$ and $4\Delta(u_i^*) < \tau^2(u_i^*)$ (P_i is an unstable node in the temporal system) the fixed point has two pairs of opposite imaginary eigenvalues (double center).

(ii) When $\tau(u_i^*) < 0$ and $4\Delta(u_i^*) < \tau^2(u_i^*)$ (P_i is a stable node in the temporal system) the fixed point has two pairs of opposite real eigenvalues (reversible bisaddle).

(iii) When $4\Delta(u_i^*) > \tau^2(u_i^*)$ (P_i is a focus in the temporal system) the fixed point has quartet of complex eigenvalues (reversible saddle bifocus).

The transition from double center to reversible saddle bifocus occurs at $4\Delta(u_i^*) = \tau^2(u_i^*)$; $\tau(u_i^*) > 0$ in a Hamiltonian Hopf bifurcation where the fixed point presents a pair of degenerate opposite imaginary eigenvalues.

The transition from reversible saddle bifocus to reversible bisaddle occurs at $4\Delta(u_i^*) = \tau^2(u_i^*)$; $\tau(u_i^*) < 0$ in a reversible BD point where the fixed point presents a degenerate pair of opposite real eigenvalues.

The fold from reversible bisaddle to center saddle occurs in a reversible Takens-Bogdanov (RTB) where the fixed point presents a degenerate zero eigenvalues and a pair of opposite real eigenvalues.

The fold from double center to center saddle configuration occurs in a reversible Takens-Bogdanov-Hopf bifurcation where the fixed point presents a degenerate zero eigenvalue and two opposite imaginary eigenvalues.

APPENDIX C: NUMERICAL METHODS

The temporal integration of the system has been performed using a pseudospectral method adapted from Ref. [52] with periodic boundary conditions on a grid with $N = 4096$ nodes, a temporal step $\Delta t = 10^{-3}$ tu, and a spatial step $\Delta x = 0.12$ su. The simulation shown in Fig. 3 has been initiated with a Gaussian on the steady P_1 solution with norm $A = 3$ and variance $\sigma = 0.3$. We initiate the simulation shown in Fig. 4 adding perturbative noise to a stable pulse for close parameter points.

The TPs have been followed with a pseudo-arclength continuation method [53,54]. The solutions are found using a regular grid with $N = 4096$ nodes, $\Delta\xi = 0.12$ su, and periodic boundary conditions. We have used an integrate-phase condition to choose between the translational equivalent solutions and select the speed c of the TP.

The stability of the TPs has been determined by a numerical diagonalization of the discretized Jacobian matrix of the TPs in the PDEs in the comoving reference frame. Using the same method we obtained the eigenvalues shown in Fig. 9(e).

[1] E. Meron, Pattern formation in excitable media, Phys. Rep. **218**, 1 (1992).
[2] A. S. Mikhailov, *Foundations of Synergetics. I. Distributed Active Systems* (Springer, Berlin, 1990).
[3] *Chemical Waves and Patterns*, edited by R. Kapral and K. Showalter (Kluwer Academic Publishers, Dordrecht, 1995).
[4] S. Alonso, M. Bär, and B. Echebarria, Nonlinear physics of electrical wave propagation in the heart: A review, Rep. Prog. Phys. **79**, 096601 (2016).
[5] J. Rinzel and G. Ermentrout, Analysis of neural excitability and oscillations, in *Methods in Neuronal Modeling*, edited by C. Koch and I. Segev (MIT Press, Cambridge,1989).
[6] E. M. Izhikevich, Neural excitability, spiking and bursting, Int. J. Bifurcation Chaos Appl. Sci. Eng. **10**, 1171 (2000).
[7] E. M. Izhikevich, *Dynamical Systems in Neuroscience* (MIT Press, Cambridge, 2007).
[8] F. Plaza, M. G. Velarde, F. T. Arecchi, S. Boccaletti, M. Ciofini, and R. Meucci, Excitability following an avalanche-collapse process, Europhys. Lett. **38**, 85 (1997).
[9] J. L. A. Dubbeldam, B. Krauskopf, and D. Lenstra, Excitability and coherence resonance in lasers with saturable absorber, Phys. Rev. E **60**, 6580 (1999).
[10] D. Gomila, M. A. Matías, and P. Colet, Excitability Mediated by Localized Structures in a Dissipative Nonlinear Optical Cavity, Phys. Rev. Lett. **94**, 063905 (2005).
[11] S. Wieczorek, B. Krauskopf, and D. Lenstra, Multipulse Excitability in a Semiconductor Laser with Optical Injection, Phys. Rev. Lett. **88**, 063901 (2002).
[12] A. Yochelis, E. Knobloch, Y. Xie, Z. Qu, and A. Garfinkel, Generation of finite wave trains in excitable media, Europhys. Lett. **83**, 64005 (2008).
[13] A. Yochelis, E. Knobloch, and M. H. Köpf, Origin of finite pulse trains: Homoclinic snaking in excitable media, Phys. Rev. E **91**, 032924 (2015).
[14] W. Gerstner and W. M. Kistler, *Spiking Neuron Models* (Cambridge University Press, Cambridge, 2002).
[15] E. Benoit, J. L. Callot, F. Diener, and M. Diener, Chasse au canard (première partie), Collectanea Mathematica **32**, 37 (1981).
[16] R. Follmann, E. Rosa Jr, and W. Stein, Dynamics of signal propagation and collision in axons, Phys. Rev. E **92**, 032707 (2015).
[17] M. A. Dahlem and S. C. Müller, Reaction-diffusion waves in neuronal tissue and the window of cortical excitability, Ann. Phys. (Leipzig) **516**, 442 (2004).
[18] K.-J. Lee, W. D. McCormick, J. E. Pearson, and H. L. Swinney, Experimental observation of self-replicating spots in a reaction–diffusion system, Nature (London) **369**, 215 (1994).
[19] F. Marino and S. Balle, Excitable Optical Waves in Semiconductor Microcavities, Phys. Rev. Lett. **94**, 094101 (2005).
[20] D. Ruiz-Reynés, D. Gomila, T. Sintes, E. Hernández-García, N. Marbà, and C. M. Duarte, Fairy circle landscapes under the sea, Sci. Adv. **3**, e1603262 (2017).
[21] C. Fernandez-Oto, D. Escaff, and J. Cisternas, Spiral vegetation patterns in high-altitude wetlands, Ecol. Complex. **37**, 38 (2019).
[22] L.-X. Zhao, K. Zhang, K. Siteur, X.-Z. Li, Q.-X. Liu, and J. van de Koppel, Fairy circles reveal the resilience of self-organized salt marshes, Sci. Adv. **7**, eabe1100 (2021).
[23] D. Ruiz-Reynés, E. Mayol, T. Sintes, I. Hendriks, E. Hernández-García, C. Duarte, N. Marbà, and D. Gomila (unpublished).
[24] M. M. Romeo and C. K. R. T. Jones, The stability of traveling calcium pulses in a pancreatic acinar cell, Phys. D (Amsterdam, Neth.) **177**, 242 (2003).
[25] A. R. Champneys, V. Kirk, E. Knobloch, B. E. Oldeman, and J. Sneyd, When Shil'nikov meets Hopf in excitable systems, J. Appl. Dyn. Syst. **6**, 663 (2007).
[26] J. Halatek and E. Frey, Rethinking pattern formation in reaction-diffusion systems, Nat. Phys. **14**, 507 (2018).
[27] F. Brauns, J. Halatek, and E. Frey, Phase-Space Geometry of Mass-Conserving Reaction-Diffusion Dynamics, Phys. Rev. X **10**, 041036 (2020).
[28] A. Arinyo-i-Prats, P. Moreno-Spiegelberg, M. A. Matias, and D. Gomila, Traveling pulses in type-I excitable media, Phys. Rev. E **104**, L052203 (2021).
[29] F. Dumortier, R. Roussarie, J. Sotomayor, and H. Zoladek, *Bifurcations of Planar Vector Fields: Nilpotent Singularities and Abelian Integrals* (Springer, Berlin, 2006).
[30] M. Or-Guil, J. Krishnan, I. G. Kevrekidis, and M. Bär, Pulse bifurcations and instabilities in an excitable medium: Computations in finite ring domains, Phys. Rev. E **64**, 046212 (2001).

[31] P. Woods and A. Champneys, Heteroclinic tangles and homoclinic snaking in the unfolding of a degenerate reversible Hamiltonian-Hopf bifurcation, Phys. D (Amsterdam, Neth.) **129**, 147 (1999).

[32] P. Coullet, C. Riera, and C. Tresser, Stable Static Localized Structures in One Dimension, Phys. Rev. Lett. **84**, 3069 (2000).

[33] M. Bär, M. Hildebrand, M. Eiswirth, M. Falcke, H. Engel, and M. Neufeld, Chemical turbulence and standing waves in a surface reaction model: The influence of global coupling and wave instabilities, Chaos **4**, 499 (1994).

[34] H. Chaté and P. Manneville, Transition to Turbulence via Spatio-Temporal Intermittency, Phys. Rev. Lett. **58**, 112 (1987).

[35] I. M. Ovsyannikov and L. P. Shil'nikov, Systems with a homoclinic curve of multidimensional saddle-focus type, and spiral chaos, Math. USSR Sb. **73**, 415 (1992).

[36] B. Sandstede and A. Scheel, Gluing unstable fronts and backs together can produce stable pulses, Nonlinearity **13**, 1465 (2000).

[37] P. Glendinning and C. Sparrow, T-points: A codimension two heteroclinic bifurcation, J. Stat. Phys. **43**, 479 (1986).

[38] P. Coullet, Localized patterns and fronts in nonequilibrium systems, Int. J. Bifurcation Chaos Appl. Sci. Eng. **12**, 2445 (2002).

[39] D. Gomila, P. Colet, and D. Walgraef, Theory for the Spatiotemporal Dynamics of Domain Walls Close to a Nonequilibrium Ising-Bloch Transition, Phys. Rev. Lett. **114**, 084101 (2015).

[40] S. Nii, The accumulation of eigenvalues in a stability problem, Phys. D (Amsterdam, Neth.) **142**, 70 (2000).

[41] J. Burke and E. Knobloch, Homoclinic snaking: Structure and stability, Chaos **17**, 037102 (2007).

[42] D. Walgraef, *Spatio-Temporal Pattern Formation: With Examples from Physics, Chemistry, and Materials Science*, Partially Ordered Systems (Springer, New York, 2012).

[43] A. R. Champneys, Homoclinic orbits in reversible systems and their applications in mechanics, fluids and optics, Phys. D (Amsterdam, Neth.) **112**, 158 (1998).

[44] M. Haragus and G. Iooss, *Local Bifurcations, Center Manifolds, and Normal Forms in Infinite-Dimensional Dynamical Systems* (Springer London, London, 2011).

[45] D. Ruiz-Reynés, L. Martín, E. Hernández-García, E. Knobloch, and D. Gomila, Patterns, localized structures and fronts in a reduced model of clonal plant growth, Phys. D (Amsterdam, Neth.) **414**, 132723 (2020).

[46] A. Yochelis, Y. Tintut, L. L. Demer, and A. Garfinkel, The formation of labyrinths, spots and stripe patterns in a biochemical approach to cardiovascular calcification, New J. Phys. **10**, 055002 (2008).

[47] D. Michaelis, U. Peschel, F. Lederer, D. V. Skryabin, and W. J. Firth, Universal criterion and amplitude equation for a nonequilibrium Ising-Bloch transition, Phys. Rev. E **63**, 066602 (2001).

[48] M. Tlidi, A. G. Vladimirov, D. Pieroux, and D. Turaev, Spontaneous Motion of Cavity Solitons Induced by a Delayed Feedback, Phys. Rev. Lett. **103**, 103904 (2009).

[49] P. V. Paulau, D. Gomila, P. Colet, M. A. Matías, N. A. Loiko, and W. J. Firth, Drifting instabilities of cavity solitons in vertical-cavity surface-emitting lasers with frequency-selective feedback, Phys. Rev. A **80**, 023808 (2009).

[50] A. Marasco, A. Iuorio, F. Cartení, G. Bonanomi, D. M. Tartakovsky, S. Mazzoleni, and F. Giannino, Vegetation pattern formation due to interactions between water availability and toxicity in plant-soil feedback, Bull. Math. Biol. **76**, 2866 (2014).

[51] A. Iuorio and F. Veerman, The influence of autotoxicity on the dynamics of vegetation spots, Phys. D (Amsterdam, Neth.) **427**, 133015 (2021).

[52] R. Montagne, E. Hernández-García, A. Amengual, and M. San Miguel, Wound-up phase turbulence in the complex Ginzburg-Landau equation, Phys. Rev. E **56**, 151 (1997).

[53] W. C. Rheinboldt, Lectures on numerical methods in bifurcation problems (Herbert B. Kelley), SIAM Rev. **30**, 677 (1988).

[54] H. D. Mittelmann, A pseudo-arclength continuation method for nonlinear eigenvalue problems, SIAM J. Numer. Anal. **23**, 1007 (1986).